Journal of Advanced Ceramics
2021, **10**(1): 49–61
https://doi.org/10.1007/s40145-020-0416-3
ISSN 2226-4108
CN 10-1154/TQ

Research Article

Effect of starting materials and sintering temperature on microstructure and optical properties of Y_2O_3:Yb^{3+} 5 at% transparent ceramics

R. P. YAVETSKIY[a,*], A. E. BALABANOV[a], S. V. PARKHOMENKO[a], O. S. KRYZHANOVSKA[a], A. G. DOROSHENKO[a], P. V. MATEYCHENKO[a], A. V. TOLMACHEV[a], Jiang LI[b], Nan JIANG[b], L. GHEORGHE[c], M. ENCULESCU[d]

[a]*Institute for Single Crystals of NAS of Ukraine*, *60 Nauky Ave.*, *Kharkiv 61072*, *Ukraine*
[b]*Key Laboratory of Transparent Opto-functional Inorganic Materials*, *Shanghai Institute of Ceramics*, *Chinese Academy of Sciences*, *Shanghai 201899*, *China*
[c]*National Institute for Laser*, *Plasma and Radiation Physics*, *Laboratory of Solid-State Quantum Electronics*, *Magurele 077125*, *Ilfov*, *Romania*
[d]*National Institute of Materials Physics*, *Magurele 077125*, *Ilfov*, *Romania*

Received: April 30, 2020; Revised: August 6, 2020; Accepted: August 25, 2020

Abstract: Y_2O_3:Yb^{3+} 5 at% ceramics have been synthesized by the reactive sintering method using different commercial yttria powders (Alfa-Micro, Alfa-Nano, and ITO-V) as raw materials. It has been shown that all Y_2O_3 starting powders consist from agglomerates up to 5–7 μm in size which are formed from 25–60 nm primary particles. High-energy ball milling allows to significantly decreasing the median particle size D_{50} below 500 nm regardless of the commercial powders used. Sintering experiments indicate that powder mixtures fabricated from Alfa-Nano yttria powders have the highest sintering activity, while $(Y_{0.86}La_{0.09}Yb_{0.05})_2O_3$ ceramics sintered at 1750 ℃ for 10 h are characterized by the highest transmittance of about 45%. Y_2O_3:Yb^{3+} ceramics have been obtained by the reactive sintering at 1750–1825 ℃ using Alfa-Nano Y_2O_3 powders and La_2O_3+ZrO_2 as a complex sintering aid. The effects of the sintering temperature on densification processes, microstructure, and optical properties of Y_2O_3:Yb^{3+} 5 at% ceramics have been studied. It has been shown that Zr^{4+} ions decrease the grain growth of Y_2O_3:Yb^{3+} ceramics for sintering temperatures 1750–1775 ℃. Further increasing the sintering temperature was accompanied by a sharp increase of the average grain size of ceramics referred to changes of structure and chemical composition of grain boundaries, as well as their mobility. It has been determined that the optimal sintering temperature to produce high-dense yttria ceramics with transmittance of 79%–83% and average grain size of 8 μm is 1800 ℃. Finally, laser emission at ~1030.7 nm with a slope efficiency of 10% was obtained with the most transparent Y_2O_3:Yb^{3+} 5 at% ceramics sintered.

Keywords: transparent ceramics; reactive sintering; microstructure; grain growth; lasing

* Corresponding author.
E-mail: yavetskiy@isc.kharkov.ua

1 Introduction

Yttrium oxide ceramics doped with trivalent ytterbium ions (Y_2O_3:Yb^{3+}) are currently investigated as promising material for the development of active media for solid-state lasers, especially for operation in high-power short-pulse generation mode [1–3]. Y_2O_3:Yb^{3+} combines good thermo-optical properties with large emission bandwidth, allowing high laser efficiency and reduced pulse duration compared to Yb^{3+}-doped yttrium aluminum garnet (YAG:Yb^{3+}). Due to the short pulse duration, high peak power, good quality of transverse beam profile, and small size, Y_2O_3:Yb^{3+} microchip lasers are of significant interest for a wide variety of applications, ranging from telemetry to laser material processing [4,5].

There are several approaches to produce transparent yttria ceramics by using hot pressing [6], hot isostatic pressing (HIP) [7–9], spark plasma sintering (SPS) [10], microwave sintering [11], or vacuum sintering [12–14]. In Ref. [6], Y_2O_3:Yb^{3+} ceramics were produced by combining hot pressing and hot isostatic pressing of co-precipitated nanopowders coated with LiF sintering aid. However, this approach is quite complicated; it is difficult to control the amount and distribution homogeneity of sintering aid used. Spark plasma sintering of nanocrystalline powders was applied to obtain Y_2O_3:Yb^{3+} ceramics with average grain size of 260 nm [10]. Moreover, laser oscillation was achieved for Y_2O_3:Yb^{3+} 10 at% ceramics. As stated by the authors, the optical and laser properties of Y_2O_3:Yb^{3+} ceramics produced by SPS are not high enough to be used for laser applications. Balabanov *et al.* [11] reported application of microwave sintering to fabricate transparent Y_2O_3:Yb^{3+} ceramics from nanopowders prepared by the high-temperature self-propagating synthesis. Despite of several advantages of microwave sintering reported (the volumetric absorption of microwave radiation, "clean" sintering conditions due to the absence of heating elements in the chamber [11]) this method is seldom used to produce optical ceramics. Summarizing, sintering using hot pressures allows decreasing the consolidation temperature and recrystallization rate due to considerable activation of volume diffusion and creep. However, the high cost of the equipment and significant operational expenses restrict the application of sintering under high pressures.

An alternative approach to fabricate Y_2O_3:Yb^{3+} laser ceramics is sintering without applying high pressures, such as vacuum sintering [12–14]. In order to increase sintering activity and reduce consolidation temperatures, nanopowders with high excess of surface energy are required. Typically, Y_2O_3:Yb^{3+} nanopowders could be obtained by co-precipitation method [15] or high-temperature self-propagating synthesis [16,17]. High surface energy of nanopowders can lead to their morphological and phase metastability (agglomeration and formation of nonequilibrium phases). For example, nanopowders obtained by co-precipitation method and subsequent annealing of the precursors have multilevel agglomeration, which significantly complicates the consolidation to a non-porous state and the formation of ceramics with adjustable microstructure [16,18].

The agglomeration of starting nanopowders could be prevented by using simple reactive sintering which provides the system additional driving force for densification. Lattice transformations occurring during the formation of Y_2O_3:Yb^{3+} solid solution from starting oxides will activate diffusion–dislocation processes, resulting in effective densification of ceramics. Consolidation at the intermediate and final sintering stages can be significantly improved by the use of sintering additives, such as ZrO_2 or La_2O_3. However, the use of high concentrations of La_2O_3 sintering additive may be accompanied by formation of cracks [19], or disorder glass-like structure [20] in ceramics. To overcome these problems, complex sintering aid La_2O_3+ZrO_2 has been utilized [21–26]. It is assumed that phase transitions during reactive sintering processes [14] and point defects formed as a result of Zr^{4+}-doping [27,28] will have synergetic effect on sintering. It should be noted that there is a lack of reports on reactive sintering of Y_2O_3:Yb^{3+} ceramics using La_2O_3+ZrO_2 complex sintering aid. Only in Ref. [25], Y_2O_3:Yb^{3+} highly-transparent ceramics have been produced by the reactive sintering using La_2O_3+ZrO_2 additive. Nevertheless, neither comprehensive study of sintering processes nor laser parameters of ceramics obtained were reported. In this work, the effect of different starting materials of yttrium oxide on formation of Y_2O_3:Yb^{3+} transparent ceramics by the reactive sintering has been studied for the first time; the evolution of the microstructure and optical properties of ceramics as a function of processing conditions are determined.

2 Experimental

2.1 Fabrication of Y_2O_3:Yb^{3+} ceramics

$(Y_{0.86}La_{0.09}Yb_{0.05})_2O_3$ and $(Y_{0.93}Yb_{0.05}La_{0.005}Zr_{0.015})_2O_3$

ceramics were obtained by the reactive sintering method. High-purity commercial powders were used as starting materials: (a) Y_2O_3 < 10 μm (99.999%, Alfa-Aesar), (b) Y_2O_3 25–50 nm (99.99%, Alfa-Aesar), (c) Y_2O_3 < 10 μm (ITO-V, Lanhit, Russia), further denoted as Alpha-Micro, Alpha-Nano, and ITO-V, respectively. Yb_2O_3 (99.99%, Alfa-Aesar) commercial powders were used as activator. La_2O_3 (99.99%, Alfa-Aesar) and ZrO_2 (99%+, US Research Nanomaterials) were used as sintering additives. The powders were weighed according to $(Y_{0.86}La_{0.09}Yb_{0.05})_2O_3$ or $(Y_{0.93}Yb_{0.05}La_{0.005}Zr_{0.015})_2O_3$ stoichiometry and ball-milled for 15 h with 10 mm zirconia balls in zirconia jar using absolute ethanol as solvent. Rotation speed was 140 rpm, and the ball to powder ratio was 7. The obtained slurry was dried at 60 ℃ for 4 h and screened through a 200-mesh sieve. The powder mixtures were then calcined at 600 ℃ for 4 h. The green bodies were prepared by uniaxial pressing and cold isostatic pressing (CIP) at P = 250 MPa, followed by annealing in air at 800 ℃. The sintering of ceramics was performed using a vacuum ($P = 10^{-3}$ Pa) furnace with tungsten heating elements in the temperature range of 1750–1850 ℃ for 10 h. After sintering, the ceramics were annealed in air at 1400 ℃ for 15 h.

2.2 Caracterization of starting nanopowders and Y_2O_3:Yb^{3+} optical ceramics

The microstructure and elemental analysis of Y_2O_3:Yb^{3+} powders and ceramics were performed by scanning electron microscopy (SEM) using a JSM-6390 LV microscope, JEOL, Japan, and Carl Zeiss Ultra 55+ microscope, Carl Zeiss, Germany, equipped with energy dispersive X-ray (EDX) detector X-Max by Oxford Instruments, UK. The particle size distributions of starting powders and powder mixtures were determined by dynamic light scattering (DLS) using Analysette 22 NanoTec plus, Fritsch GmbH, Germany. The measurements of each sample were conducted in Nano mode (0.01–45.00 μm) under ultrasound for 30 s. Dilatometric studies of powders were performed by a constant rate of heating sintering using a Netzsch 402 ED differential dilatometer up to 1500 ℃ at a heating rate of 10 ℃/min.

The X-ray diffraction (XRD) studies of initial nanopowders were performed on a Siemens D500 powder diffractometer in Bragg–Brentano geometry in the angular range $5° < 2\theta < 90°$ (Cu Kα radiation). The X-ray diffraction pattern of lanthanum boride (LaB_6) powders, recorded under similar conditions, was used as a standard X-ray diffraction pattern for determining the instrumental parameters of the line profile. The XRD patterns were analyzed by using WinLOTR and FullProg software using the Voigt function to describe the profile. Phase identification was performed using the PDF-1 JCPDS X-ray database of the EVA survey system, which is part of the diffractometer software.

Y_2O_3:Yb^{3+} ceramics were polished at laser grade using a PM5 Precision Lapping and Polishing Machine (Logitech, Scotland, UK). The average grain size of ceramics was calculated using the secant method. The samples were thermally etched at 1450 ℃ for 15 h in order to reveal grain boundaries. The statistical sampling for each specimen was at least 300 grains. The transmittance spectra of Y_2O_3:Yb^{3+} ceramics with the thickness of 1.5 mm were measured in the 0.2–2.5 μm range using a Carry 500 UV–VIS–NIR spectrometer. The infrared spectra were recorded with a Scanning Microscope Spotlight 400 imaging system (Perkin Elmer) coupled with a Spectrum 100 FTIR (Fourier transform infrared spectroscopy) spectrometer, in transmission mode, between 4000 and 500 cm^{-1} (2500–20,000 nm), each spectrum having a resolution of 4 cm^{-1}.

The laser experiments on Y_2O_3:Yb^{3+} ceramics were performed under pumping at ~970 nm with a fiber-coupled diode laser (Limo Co., Germany). The fiber end (of 100 μm diameter and numerical aperture NA = 0.22) was imaged (1:1 ratio) into ceramic sample using a pair of collimating and focusing achromatic lenses, both of 40 mm focal length. The diode laser was operated in quasi-continuous-wave mode with pump pulses of 1 ms duration at 5-Hz repetition rate.

3 Results and discussion

3.1 Selection of starting materials for solid-state sintering of Y_2O_3:Yb^{3+} ceramics

Fabrication of Y_2O_3:Yb^{3+} ceramics with optical quality puts forward special requirements to the particle size, phase, and chemical composition of the starting powders. The average particle size, particle size distribution, shape, and agglomeration degree have a crucial effect on the sinterability of powders, as well as on the microstructure of final ceramics. Let us consider the correlation between powder parameters, solid-state sintering conditions, and laser characteristics of ceramics. In order to select the starting materials suitable for obtaining of Y_2O_3:Yb^{3+} ceramics by the solid-state

sintering method, three types of commercial powders were investigated: Alpha-Micro, Alpha-Nano, and ITO-V. Figure 1 presents the FESEM images of starting Y_2O_3 powders. The average aggregate size of Alpha-Micro and ITO-V yttria starting powders is of about 5–7 microns (Figs. 1(a) and 1(c)), which generally corresponds to the manufacturers' data (< 10 μm). According to SEM results, agglomerates of yttrium oxide are formed from primary particles of isometric shape from the size range of 40–60 nm (Figs. 1(a) and 1(c)). The aggregates of yttria particle have a complex hierarchy structure and contain a large number of cracks between adjacent blocks. This structure is typical for the powders obtained by chemical precipitation method, and the presence of cracks is due to the removal of gaseous products during precursor crystallization. For nanoscale yttrium oxide (Fig. 1(b)), the average size of the agglomerates also reaches few microns, but the shape of the aggregates is significantly different. Alpha-Nano Y_2O_3 powders are formed by lamellar particle aggregates of rhombic shape with a typical thickness of 25–50 nm. Similar particles can be obtained by the chemical co-precipitation method at large supersaturation values of mother solution [29].

According to dynamic light scattering (DLS) results, Alfa-Micro and ITO-V Y_2O_3 powders have a similar particle size distribution (Figs. 1(d) and 1(f)). They contain particles with an average particle size of about 100 nm and several pronounced fractions of agglomerates from the 2–20 μm range, as confirmed by SEM (Fig. 1). The mean diameter D_{50} was found to be 0.2 μm for Alfa-Micro powders and 6 μm for ITO-V, indicating much harder agglomeration. Alfa-Nano powders are characterized by the presence of a fraction of isolated nanoparticles less than 50 nm, as well as agglomerates reaching 5–12 μm (Fig. 1(e)). The medium value of the particle size distribution D_{50} is 12 μm.

According to XRD patterns (Fig. 2), Alpha-Micro, Alpha-Nano, and ITO-V powders are single-phase cubic yttrium oxide, and no secondary phases were detected. The lattice parameters calculated using the Rietveld refinement are given in Table 1. The crystallite size of the starting yttrium oxide powders lies within the 25–60 nm range. Alpha-Nano Y_2O_3 powders are characterized by the smallest average crystallite size and the largest lattice parameter. According to XRD data all the studied powders are nanocrystalline (Table 1). Agglomeration degree of powders was roughly estimated by using D_{50}/L ratio, where L is the crystallite size. It was determined that $D_{50}/L \approx 3$ and 139 for Alpha-Micro and ITO-V powders, respectively. Alpha-Nano yttria is characterized by agglomeration degree of 461, which does not seem to be adequate due to the presence of a fine-dispersed fraction on the particle size distribution and fine hierarchic structure revealed by SEM (Fig. 1(b)).

SEM of ball-milled $0.86Y_2O_3{\cdot}0.09La_2O_3{\cdot}0.05Yb_2O_3$ powder mixtures prepared using different starting yttria powders are shown in Fig. 3. The mixture obtained using and ITO-V powders contains hard agglomerates reaching 2 μm in size, which were not crushed during

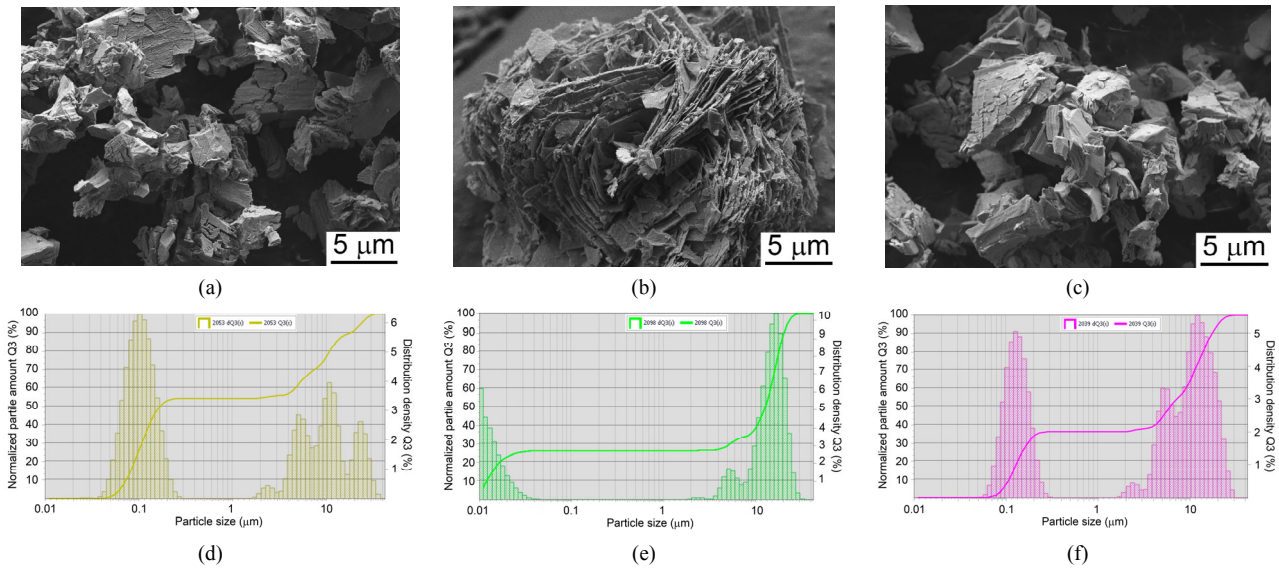

Fig. 1 SEM (a–c) and particle size distribution obtained by DLS method (d–f) of Alpha-Micro (a, d), Alpha-Nano (b, e), and ITO-V (c, f) commercial Y_2O_3 powders.

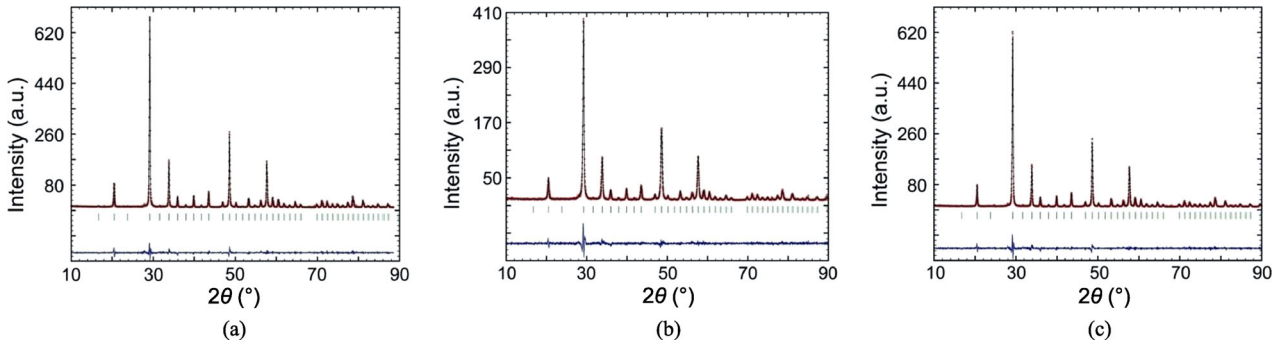

Fig. 2 X-ray diffraction patterns of Alpha-Micro (a), Alpha-Nano (b), and ITO-V (c) commercial Y_2O_3 powders.

Table 1 Phase composition of the starting Y_2O_3 powders

Sample	Phase	Phase content (wt%)	Average crystallite size *L* (nm)	Lattice parameter (Å)
Alpha-Micro	Y_2O_3	100	58	*a*=10.60027(11)
Alpha-Nano	Y_2O_3	100	26	*a*=10.60309(18)
ITO-V	Y_2O_3	100	43	*a*=10.59976(13)

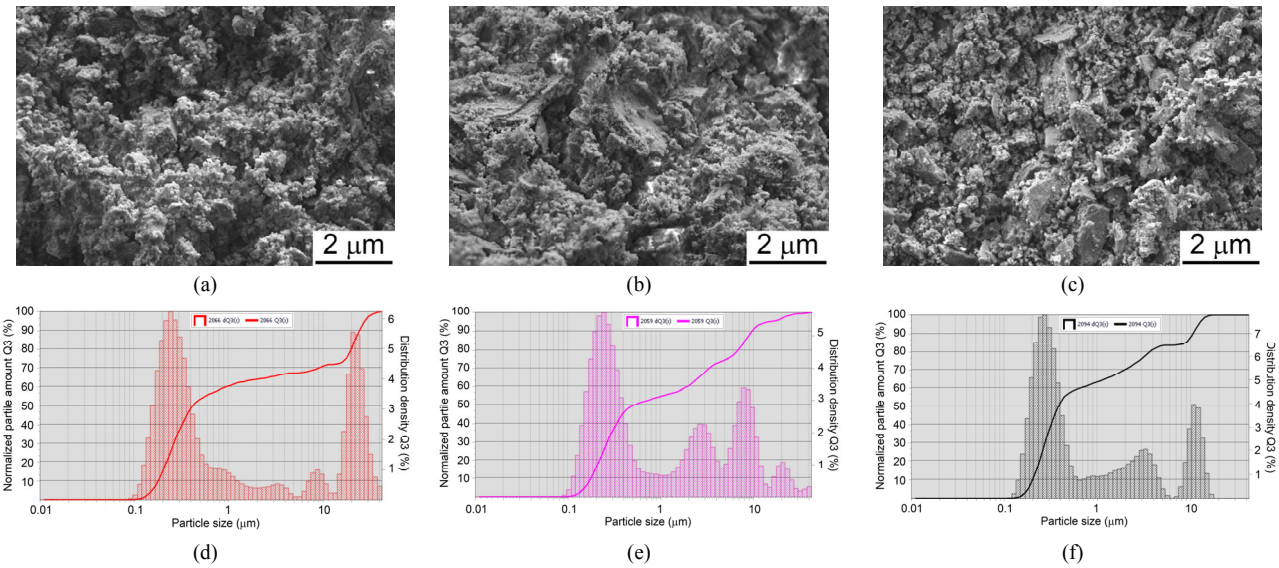

Fig. 3 SEM (a–c) and particle size distribution (d–f) of $0.86Y_2O_3{\cdot}0.09La_2O_3{\cdot}0.05Yb_2O_3$ powder mixtures prepared using Alpha-Micro (a, d), Alpha-Nano (b, e), and ITO-V (c, f) Y_2O_3 powders.

high-energy ball-milling process (Fig. 3(c)). The powder mixtures obtained using Alpha-Micro and Alpha-Nano Y_2O_3 powders are the most homogeneous, while the smallest average particle size less than 100 nm was revealed for Alpha-Nano powders (Fig. 3(b)). This indicates that agglomerates in starting Alfa-Nano yttria are soft.

Particle size distributions of all the powder mixtures studied show the presence of a main fraction with a particle size of about 0.2 μm; polymodal fractions of agglomerates ranging from 1–5 to 40 μm were also detected (Figs. 3(d) –3(f)). It seems that the agglomerates revealed by DLS have completely different structure. While agglomeration of ITO-V powder mixtures comes from secondary aggregates survived after ball milling (Fig. 3(c)), agglomeration of Alpha-Nano powders is apparently explained by an interaction of nanoparticles in suspension during DLS study. Alpha-Micro mixtures show intermediate behavior between the cases described. The D_{50} parameter for all the mixtures studied lies within the 0.4–0.5 μm range.

Densification behavior of yttria powders was studied by two different sintering methods (constant rate of heating sintering and vacuum sintering) using $(Y_{0.86}La_{0.09}Yb_{0.05})_2O_3$

model composition, possessing excellent sinterability [11,12,14–16]. $0.86Y_2O_3{\cdot}0.09La_2O_3{\cdot}0.05Yb_2O_3$ powder mixtures prepared by ball milling of different starting yttria powders were compacted by cold isostatic pressing under pressure of 250 MPa and sintered at the constant heating rate of 10 ℃/min. The density of sintered specimens as a function of the sintering temperature is given in Fig. 4(a). The relative density of all the green bodies studied was ~55% of the theoretical one, while the character of density increase with temperature was quite different for various nanopowders. The consolidation of powder mixtures obtained from micron-sized yttrium oxide powder starts at 1200 ℃ (Fig. 4(a), curves 1 and 3). $0.86Y_2O_3{\cdot}0.09La_2O_3{\cdot}0.05Yb_2O_3$ powder mixture obtained from nanocrystalline powders begins to densify at much lower temperature of 850 ℃ (Fig. 4(a), curve 2). After reaching the temperature of 1500 ℃, $0.86Y_2O_3{\cdot}0.09La_2O_3{\cdot}0.05Yb_2O_3$ powder mixtures obtained by using Alpha-Micro, Alpha-Nano, and ITO-V yttrium oxide powders possess relative densities of 65%, 78%, and 70%, respectively. Beneficial sintering activity of powder mixture prepared from Alpha-Nano powders originates from excellent dispersion, weak agglomeration state, and small size of the nanoparticles (Fig. 3(b)).

Figure 4(b) shows the shrinkage rate and the sintering activity of $0.86Y_2O_3{\cdot}0.09La_2O_3{\cdot}0.05Yb_2O_3$ powder mixtures prepared using different starting yttria powders. The sinterability of powder mixtures prepared from Alpha-Micro and ITO-V micron powders, measured at 1450 ℃, is $\mathrm{d}(\Delta\rho/\rho_0)\mathrm{d}t \approx 0.15$. This is about a half of the value of Alpha-Nano powder mixture ($\mathrm{d}(\Delta\rho/\rho_0)\mathrm{d}t \approx 0.3$). Moreover, densification rate of powder mixture prepared using ITO-V micron powders shows a decrease after reaching the temperature of 1420 ℃. This can be explained by microstructural features of the powders after ball milling (Fig. 3). Powder mixtures prepared from ITO-V micron powders contain residual agglomerates up to 2 μm in dimension survived after milling process (Fig. 3(c)). As a result, green bodies prepared from such a powder will have local density variations, and will be characterized by non-uniform sintering. At the first stage sintering of individual particles within agglomerates occurs, while at the second stage sintering of large agglomerates begins. Despite permanent increase of density of ITO-V ceramics, shrinkage rate decreases due to local inhomogenities of particles packing (Fig. 4(b), curve 3). In contrast, ball-milled batches prepared from Alpha-Micro and

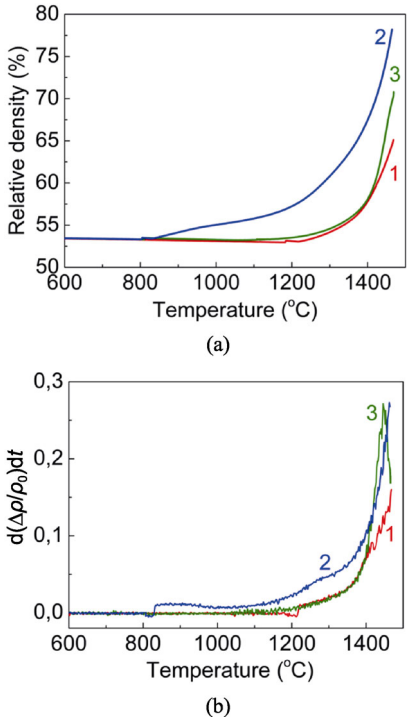

Fig. 4 Shrinkage curves (a) and shrinkage rates (b) of $0.86Y_2O_3{\cdot}0.09La_2O_3{\cdot}0.05Yb_2O_3$ powder mixtures prepared using Alpha-Micro (1), Alpha-Nano (2), and ITO-V (3) Y_2O_3 powders.

Alpha-Nano powders are well dispersed and quite homogenous, no agglomerates were detected (Figs. 3(a) and 3(b)). Consequently, green bodies fabricated from the latter powders have relatively high sintering activity and exhibit a further tendency to densification even the temperature of 1500 ℃ is reached. Taking into account the microstructure, particle size distribution, and sinterability of powder mixtures obtained from different yttria sources it was shown that Alfa-Nano have the highest sintering activity. Moreover, it could be assumed that agglomerates revealed by DLS in ball-milled Alpha-Nano powders are soft and could be broke down during cold pressing.

Finally, $0.86Y_2O_3{\cdot}0.09La_2O_3{\cdot}0.05Yb_2O_3$ powder mixtures prepared using different starting yttria powders were studied by vacuum sintering. The ball milled powders were compacted by cold isostatic pressing and sintered in a vacuum furnace with tungsten heating elements at 1750 ℃ for 10 h. After that, ceramics were annealed at 1400 ℃ for 15 h in air in order to remove color centers formed in oxygen-deficient atmosphere. However, even after annealing ceramics have a light gray or yellow color, indicating that color centers were not completely removed (Fig. 5).

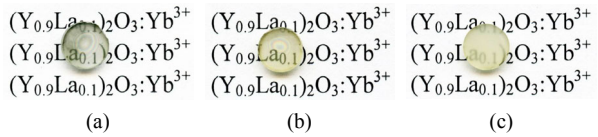

Fig. 5 $(Y_{0.86}La_{0.09}Yb_{0.05})_2O_3$ ceramics prepared using Alpha-Micro (a), Alpha-Nano (b), and ITO-V (c) Y_2O_3 powders by vacuum sintering at T = 1750 ℃ for 10 h.

$(Y_{0.86}La_{0.09}Yb_{0.05})_2O_3$ ceramics obtained by using ITO-V powders were virtually opaque, while the ceramics produced from Alpha-Micro and Alpha-Nano powders were transparent (Figs. 5(a) and 5(b)). It should be noted that the results of vacuum sintering (Fig. 5) and constant rate of heating sintering of yttria ceramics (Fig. 4) show excellent correlation.

The in-line optical transmittance spectra of $(Y_{0.86}La_{0.09}Yb_{0.05})_2O_3$ ceramics measured on polished 1.5 mm thick samples are presented in Fig. 6. Yttria ceramics are transparent from UV to near IR wavelength range (the band gap width of Y_2O_3 is of about 6 eV [30]). The absorption lines in the 850–1050 nm range were assigned to 4f–4f transitions of Yb^{3+} ions. The transmittance of $(Y_{0.86}La_{0.09}Yb_{0.05})_2O_3$ ceramics prepared from Alpha-Micro, Alpha-Nano, and ITO-V Y_2O_3 powders reaches 40%, 45%, and 5% at λ = 1100 nm, correspondingly. The most transparent $(Y_{0.86}La_{0.09}Yb_{0.05})_2O_3$ ceramics, obtained by using Alfa-Nano raw materials, are characterized by the in-line optical transmittance of about 45% (Fig. 6, curve 2), which is 55% from the theoretical value. Thus, Alfa-Nano powders can be consolidated into transparent ceramics using lanthanum oxide as the sintering additive. Taking into account the results of complex studies of the effect of starting Y_2O_3 powders on sinterability of yttria ceramics, Alfa-Nano yttria powders were chosen for further experiments.

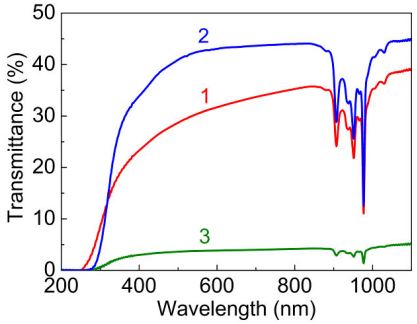

Fig. 6 In-line optical transmittance spectra of $(Y_{0.86}La_{0.09}Yb_{0.05})_2O_3$ ceramics, sintered at T = 1750 ℃ using Alpha-Micro (1), Alpha-Nano (2), and ITO-V (3) Y_2O_3 powders.

3.2 Optimization of processing conditions of $(Y_{0.93}Yb_{0.05}La_{0.005}Zr_{0.015})_2O_3$ ceramics

The general trend in development of oxide optical ceramics is to decrease an amount of sintering additives used [31]. This concept allows to prevent color centers formation, precipitation of secondary phases, segregation of impurities along grain boundaries, as well as to improve optical properties of ceramics and their functional response. While sintering of optical grade YAG:Yb^{3+} ceramics without sintering aid was recently reported [31], this approach is still very challenging, especially for the reactive sintering method. Fabrication of yttria ceramics with La_2O_3+ZrO_2 sintering aid has been described in many papers [21–26]. However, most of the authors use high concentration of sintering additives (6–13 at%). In the second part of our work we report the synthesis of yttrium oxide ceramics using complex sintering additives La_2O_3+ZrO_2 with the lowest total concentration ever reported (2 at%) [32]. The powder mixtures were obtained according to Ref. [32], using Alpha-Nano Y_2O_3 powders as starting material. Figure 7 shows the micrograph of $0.93Y_2O_3{\cdot}0.005La_2O_3{\cdot}0.05Yb_2O_3{\cdot}0.015Zr_2O_3$ powder mixture after high-energy ball milling. It can be seen that the milling allows to almost completely remove the micron aggregates and to displace the average particle size of the mixture into the submicron range. The ball-milled powders are characterized by a fine structure and the average size of aggregates is 300–450 nm, which indicates the high homogeneity of the powders after ball milling. Aggregates and agglomerates with size in micron range were not detected.

Figure 8 shows photographs of polished samples of $(Y_{0.93}Yb_{0.05}La_{0.005}Zr_{0.015})_2O_3$ transparent ceramics obtained by vacuum sintering in T = 1750–1825 ℃ temperature range. It can be seen that the samples are

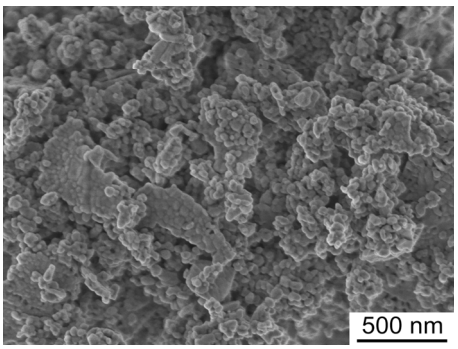

Fig. 7 SEM image of $0.93Y_2O_3{\cdot}0.005La_2O_3{\cdot}0.05Yb_2O_3{\cdot}0.015Zr_2O_3$ powder mixture after ball milling for 15 h.

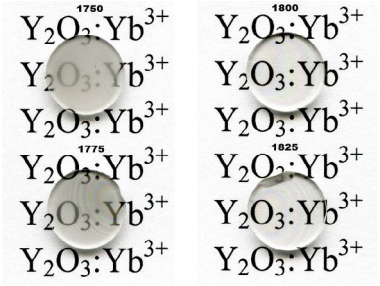

Fig. 8 $(Y_{0.93}Yb_{0.05}La_{0.005}Zr_{0.015})_2O_3$ optical ceramics obtained by vacuum sintering for 10 h at different temperatures and annealed in air at 1400 ℃ for 15 h.

characterized by different degree of transparency. The optical transmission increases significantly with the sintering temperature rise from 1750 to 1800–1825 ℃.

Figure 9 shows SEM micrographs of thermally etched surfaces of $(Y_{0.93}Yb_{0.05}La_{0.005}Zr_{0.015})_2O_3$ ceramics. The ceramics obtained at 1750 ℃ are characterized by a significant number of residual pores while the grain shape being fuzzy and "rounded" (Fig. 9(a)). It can be argued that the sintering processes are not completed; the dense microstructure of ceramics is not fully formed resulting in relative low density and optical transmittance. Sintering at T = 1775 ℃ has practically no effect on the microstructure of $(Y_{0.93}Yb_{0.05}La_{0.005}Zr_{0.015})_2O_3$ ceramics (Fig. 9(b)). The residual pores are still present, but grain boundaries become sharper. Increasing the sintering temperature to T = 1800 ℃ leads to formation of more homogeneous microstructure and increases the average grain size due to intensification of the diffusion processes and mass transfer. Ceramics sintered at T = 1800 ℃ possess almost pore-free microstructure, and mainly flat grain boundaries are observed (Fig. 9(c)). This trend also persists in $(Y_{0.93}Yb_{0.05}La_{0.005}Zr_{0.015})_2O_3$ ceramics obtained by vacuum sintering at T = 1825 ℃ (Fig. 9(d)).

In order to reveal possible compositional inhomogeneities the sintered yttria ceramics were studied by STEM correlated with EDS, which provides a resolution of several nanometers, depending on the local sample thickness. Elemental maps in areas containing grain boundaries were obtained. STEM image and elemental mapping of constituent elements of $(Y_{0.93}Yb_{0.05}La_{0.005}Zr_{0.015})_2O_3$ ceramics sintered at 1800 ℃ are shown in Fig. 10. It can be seen that ceramics are characterized by homogenous microstructure, and the grain boundaries are uniform and clear without any secondary or glassy phases. According to the EDS analysis results, the elemental composition of the ceramics within the grains and at grain boundaries is identical within the quantification errors. No segregation of Yb^{3+}, La^{3+}, and Zr^{4+} dopants along the grain boundaries was

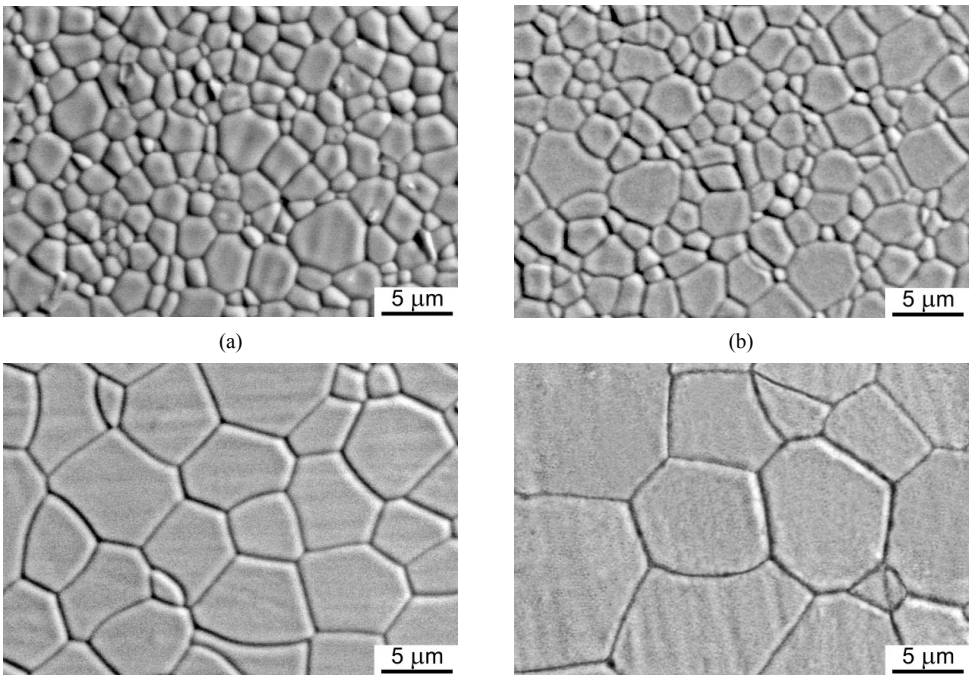

Fig. 9 SEM images of $(Y_{0.93}Yb_{0.05}La_{0.005}Zr_{0.015})_2O_3$ ceramics obtained by vacuum sintering at T = 1750 ℃ (a), 1775 ℃ (b), 1800 ℃ (c), and 1825 ℃ (d) for 10 h.

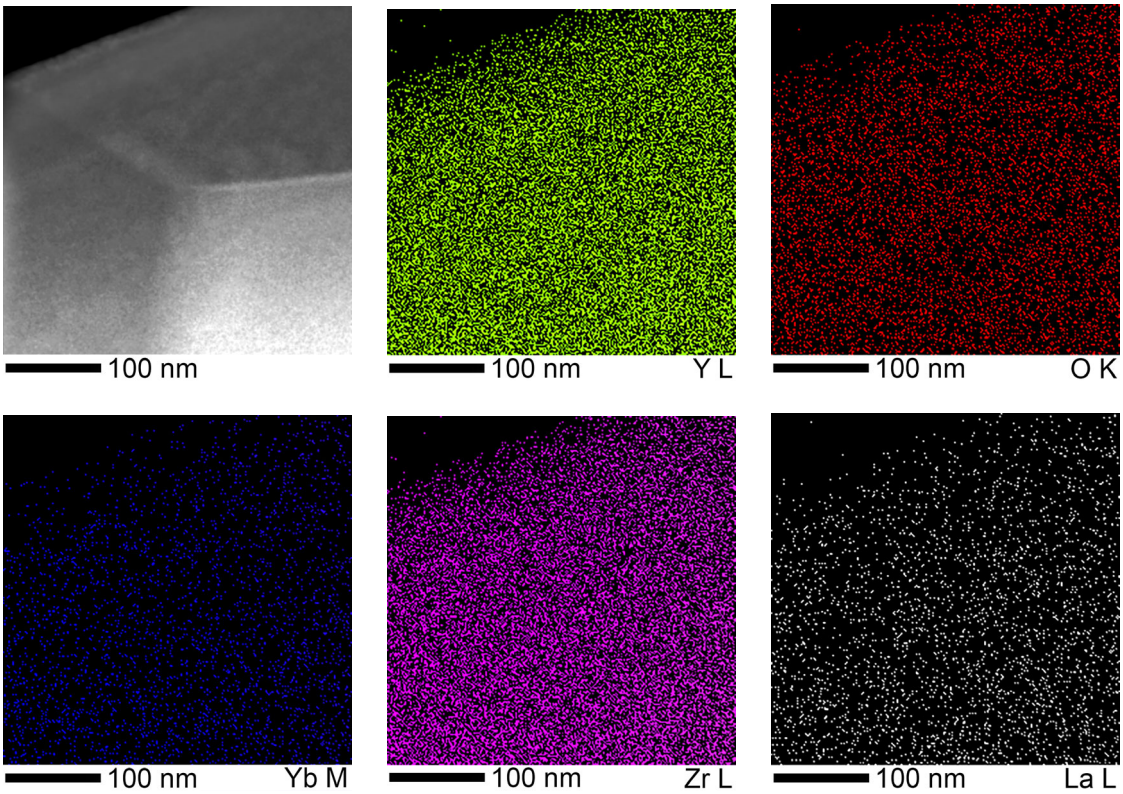

Fig. 10 STEM image and elemental mapping of $(Y_{0.93}Yb_{0.05}La_{0.005}Zr_{0.015})_2O_3$ ceramics sintered at 1800 ℃ for 10 h.

detected, indicating high structural and compositional homogeneity of $(Y_{0.93}Yb_{0.05}La_{0.005}Zr_{0.015})_2O_3$ ceramics at micro- and nanoscale (Figs. 9 and 10).

The grain size distribution of $(Y_{0.93}Yb_{0.05}La_{0.005}Zr_{0.015})_2O_3$ ceramics sintered at different temperatures is shown in Fig. 11. The ceramics synthesized at temperatures below 1800 ℃ are characterized by a narrow one-modal grain size distribution. The average grain size of yttria ceramics sintered at T = 1750 ℃ and T = 1775 ℃ is 2.8 and 2.9 μm, respectively (Figs. 11(a) and 11(b)). In the sintering temperature range of 1800–1825 ℃ the grain size dispersion increases significantly, the average grain size being 8.1 and 11.0 μm (Figs. 11(c) and 11(d)). Such a step-wise change in the grain size distribution of ceramics with the sintering temperature may be due to different grain boundary mobility [27].

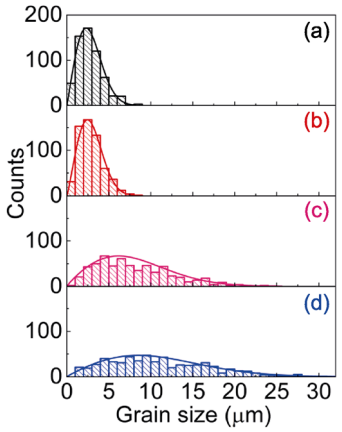

Fig. 11 Grain size distributions of $(Y_{0.93}Yb_{0.05}La_{0.005}Zr_{0.015})_2O_3$ ceramics sintered at T = 1750 ℃ (a), 1775 ℃ (b), 1800 ℃ (c), and 1825 ℃ (d) for 10 h.

The optical transmittance spectra of $(Y_{0.93}Yb_{0.05}La_{0.005}Zr_{0.015})_2O_3$ ceramics sintered at different temperatures are shown in Fig. 12. The absorption lines observed in the 850–1050 nm range correspond to intra-configuration f–f transitions of Yb^{3+} ions. We have not detected any absorption band attributed to Yb^{2+} ions. The optical transmittance of $(Y_{0.93}Yb_{0.05}La_{0.005}Zr_{0.015})_2O_3$ ceramics increases with the sintering temperature, and then slightly decreases when the obtaining temperature reaches 1825 ℃. It seems that at T = 1825 ℃ grain growth (non-densifying mechanism) becomes more pronounced as compared to pore removal (densification). That means ceramic sample sintered in these conditions has higher residual porosity. The ceramics synthesized at T = 1800 ℃ possess much better optical homogeneity; the transmittance is 63% at λ = 400 nm, 79% at 1050 nm, and 83% at 5000 nm

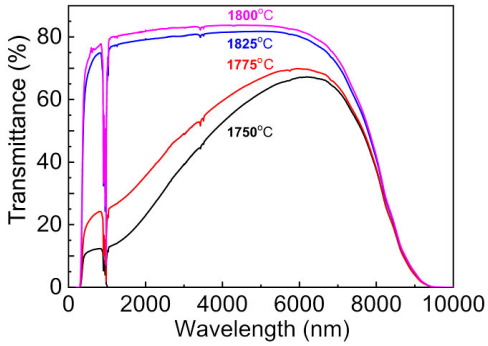

Fig. 12 Optical transmittance spectra of 1.5 mm thick $(Y_{0.93}Yb_{0.05}La_{0.005}Zr_{0.015})_2O_3$ ceramics sintered at different temperatures.

(Fig. 12). The transparency of ceramics was found to be in a good agreement with their microstructural features (Fig. 9). Thus, the optimal sintering temperature to obtain near pore-free $(Y_{0.93}Yb_{0.05}La_{0.005}Zr_{0.015})_2O_3$ ceramics is $T = 1800$ ℃.

Let us consider the effect of sintering aid and sintering temperature on the microstructure and optical properties of $(Y_{0.93}Yb_{0.05}La_{0.005}Zr_{0.015})_2O_3$ ceramics. Y^{3+} cations occupy two crystallographic positions in Y_2O_3 structure with 24*d* and 8*b* symmetry (in the Wyckoff notation [33]). 8*b* position has larger volume and is centrosymmetric, while 24*d* position has a smaller volume and lack of the center of symmetry. The introduction of isovalent lanthanum and ytterbium ions into Y_2O_3 is accompanied by formation of La_Y^X and Yb_Y^X point defects, respectively. The insertion of zirconium ions (Zr^{4+}) requires charge compensation according to the following mechanisms [28]:

$$2ZrO_2 + 2Y_Y^X \Leftrightarrow 2Zr_Y^{\bullet} + O_i'' + Y_2O_3 \quad (1)$$

$$3ZrO_2 + 4Y_Y^X \Leftrightarrow 3Zr_Y^{\bullet} + V_Y''' + 2Y_2O_3 \quad (2)$$

Zr^{4+} ions, most probably, substitute Y^{3+} ions in 24*d* noncentrosymmetric position according to Eq. (1), and an interstitial oxygen ion is formed as a charge compensator [19]. The formation of such a defect is accompanied by a decrease in the free energy of the system and leads only to a slight change of Y_2O_3 unit cell volume. It should be noted that the energy difference between (1) and (2) mechanisms is less than 1 eV [28]. According to Ref. [27], the grain boundary mobility in Y_2O_3 is controlled by cation diffusivity by interstitial mechanism, which is enhanced by the presence of oxygen vacancies and suppressed by the presence of oxygen interstitials. Doping yttria by non-isomorphic cations enhances concentration of peculiar defects, and thus, affects the grain boundary mobility and densification.

Given the above, the following sintering mechanism of $(Y_{0.93}Yb_{0.05}La_{0.005}Zr_{0.015})_2O_3$ ceramics could be proposed. First, Zr^{4+} reduces the grain boundary mobility of yttria due to the formation of charged oxygen interstitial ions [27]. Second, according to Figs. 9(a) and 9(b), 1.5 at% of Zr^{4+} ions prevents grain coarsening of $(Y_{0.93}Yb_{0.05}La_{0.005}Zr_{0.015})_2O_3$ ceramics sintered at 1750–1775 ℃; the average grain size is below 3 μm (Figs. 11(a) and 11(b)). Increasing the sintering temperature to 1800 and 1825 ℃ leads to a remarkable growth of average grain size up to 25–30 μm (Figs. 11(c) and 11(d)), while grain size distribution becomes broadened. This testifies that Zr^{4+} ions do not impede recrystallization any more. The enhanced grain boundary mobility originates, probably, due to the contribution of other trivalent additives (La^{3+}, Yb^{3+}). It was reported that yttria doping by trivalent dopants, in principle, should have no effect on grain boundary mobility. However, the trivalent dopants could increase the grain boundary mobility due to a slight distortion of the lattice [27]. Growth the sintering temperature from 1500 to 1650 ℃ results in an order of magnitude higher grain boundary mobility of Y_2O_3:Yb^{3+} 1 at% and Y_2O_3:La^{3+} 1 at% [27]. Taking into account that the sintering temperature in our study reaches 1825 ℃, the increase of grain boundary mobility could be even more pronounced.

Non-monotonic change of the average grain size of $(Y_{0.93}Yb_{0.05}La_{0.005}Zr_{0.015})_2O_3$ ceramics with the sintering temperature (Fig. 13) can be described in the framework of the theory of grain boundary complexions [34]. "Grain boundary complexion" is being used to refer to groups of grain boundaries, which are thermodynamically stable phases possessing distinct structures and compositions different from any bulk phases [35]. The ceramics obtained at the temperatures of 1750 ℃ and 1775 ℃ have almost the same average grain size of about 3 μm. A further growth of the sintering temperature from 1800 to 1825 ℃ leads to an increase in grain size up to 8 and 11 μm, respectively (Fig. 13). According to Ref. [34], such a step-wise behavior corresponds to a first-order complexion transition, which is accompanied by a sharp increase in grain boundary mobility. A similar transition was recently observed for Y_2O_3:Yb^{3+},Er^{3+} ceramics at much lower temperatures 1450–1490 ℃ [36] (see Fig. 13). It seems that increasing the sintering temperature changes

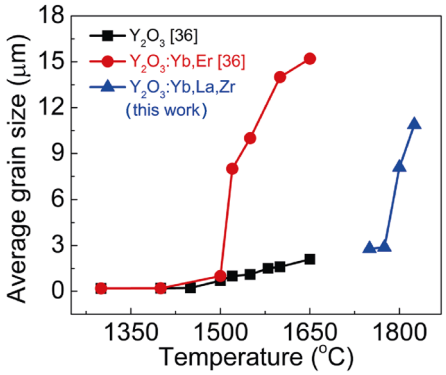

Fig. 13 Effect of the sintering temperature on the average grain size of Y_2O_3 ceramics vacuum sintered for 10 h.

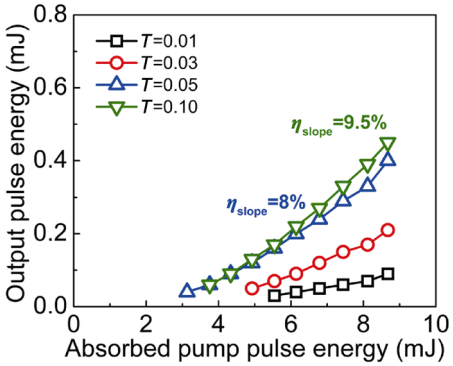

Fig. 14 Laser pulse energy (E_p) versus the pump pulse absorbed energy (E_{abs}) for $(Y_{0.93}Yb_{0.05}La_{0.005}Zr_{0.015})_2O_3$ ceramics vacuum sintered at T = 1800 ℃ for 10 h. The solid lines are linear fits of the experimental data.

structure and chemical composition of grain boundaries, which reduce the average grain boundary energy and increase the grain boundary mobility of Zr^{4+}-doped yttria ceramics. Thus, it can be assumed that the temperature shift of complexion transition to the higher temperatures for $(Y_{0.93}Yb_{0.05}La_{0.005}Zr_{0.015})_2O_3$ ceramics in comparison with Y_2O_3:Yb^{3+},Er^{3+} ceramics is caused by Zr^{4+}-doping. However, in Ref. [36] it was pointed that no systematic correlation existed between the Yb/Er dopant concentration and complexion transition temperature, though differently Yb/Er codoped Y_2O_3 specimens displayed similar jumps in grain size within this temperature range. Thus, the effect of dopant concentration on the complexion transition temperature should be clarified in future research.

$(Y_{0.93}Yb_{0.05}La_{0.005}Zr_{0.015})_2O_3$ ceramic sample having the best optical transmittance (sintered at T = 1800 ℃) was tested as active laser medium under diode laser pumping (Fig. 14). Ceramics with thickness of 1.36 mm were fixed in an optical-claw and no cooling was provided. A short linear plane-plane resonator was built (less than 10 mm in length). Out-coupling mirrors (OCM) with transmission T = 0.01, 0.03, 0.05, and 0.10 in the 1020–1080 nm wavelength range were used to extract the laser radiation from the optical resonator. Laser emission at ~1030.7 nm under quasi-continuous-wave diode pumping was achieved. Figure 14 presents the laser pulse energy, E_p, versus the pump pulse absorbed energy, E_{abs}. As can be observed, the highest slope efficiencies are obtained for the OCM with higher transmissions. When the OCM with T = 0.10 was used, the absorption efficiency was found to be $\eta_a \approx 47\%$ and the highest slope efficiency η_{sa} (with respect to the absorbed pump pulse energy) was achieved, $\eta_{sa} \approx 10\%$. The laser yielded pulses with maximum energy E_p = 0.45 mJ for E_{abs} = 8.82 mJ. The slope efficiency value obtained in these preliminary laser experiments is slightly below [37] or comparable with other values reported in the literature [7–9]. Anyway, some experimental conditions (the design of the laser resonator, the pumping wavelength, the sample thickness, etc.) must be optimized to enhance the laser performances of $(Y_{0.93}Yb_{0.05}La_{0.005}Zr_{0.015})_2O_3$ ceramics.

4 Conclusions

The effects of starting materials and processing conditions on the microstructure and optical properties of Y_2O_3:Yb^{3+} 5 at% ceramics have been studied. According to XRD and SEM data, Alpha-Micro, Alpha-Nano, and ITO-V starting yttria powders are nanocrystalline, but have fundamentally different agglomeration degree. Commercial Y_2O_3 powders have been found to consist from three-dimensional agglomerates of complex hierarchies with dimension up to 5–7 μm, which are formed from 25–60 nm primary particles. At the same time, Alpha-Nano powders have the highest sintering activity among the starting powders studied. Vacuum sintering experiments demonstrate that Y_2O_3:Yb^{3+} 5 at% ceramics produced from Alfa-Nano yttria powders possess the highest in-line optical transmittance of about 45%, which is of about 55% of the theoretical value.

It has been shown that the sintering temperature in the 1750–1825 ℃ range has great influence on the microstructure and optical properties of yttria ceramics of $(Y_{0.93}Yb_{0.05}La_{0.005}Zr_{0.015})_2O_3$ model composition.

The optical transmittance of the ceramics, as well as the grain size, increases significantly with the sintering temperature growing from 1750 to 1800–1825 ℃. The step-wise change of the average grain size with sintering temperature can be attributed to a first-order complexion transition, which is accompanied by a sharp increase in grain boundary mobility. Ceramics synthesized at T = 1800 ℃ are characterized by the highest optical homogeneity, the optical transmittance being 63% at 400 nm, 79% at 1050 nm, and 83% at 5000 nm. Finally, preliminary laser experiments on the most transparent Y_2O_3:Yb^{3+} 5 at% ceramics have been performed under diode pumping at ~970 nm. The slope efficiency η_{sa} ~10% was obtained for the OCM with T = 0.10. Further experiments concerning the laser performances are currently undertaken.

Acknowledgements

This work was supported by the National Academy of Sciences of Ukraine by the budget programs "Support for the development of priority areas of scientific research" (KPKVK 6541230). The authors are grateful to Dr. Vyacheslav Baumer from the "SSI Institute for Single Crystals" of NAS of Ukraine, Kharkiv, Ukraine, Dr. Andrei Kuncser from the National Institute of Materials Physics, Bucharest, Romania, and to Dr. Nicolaie Pavel and Dr. Gabriela Croitoru from the National Institute for Laser, Plasma and Radiation Physics, Magurele, Romania, for their help in the characterization of the ceramic samples and the fruitful discussions of the experimental results.

References

[1] Kong J, Lu J, Takaichi K, *et al*. Diode-pumped Yb:Y_2O_3 ceramic laser. *Appl Phys Lett* 2003, **82**: 2556–2558.

[2] Shirakawa A, Takaichi K, Yagi H, *et al*. Diode-pumped mode-locked Yb^{3+}:Y_2O_3 ceramic laser. *Opt Express* 2003, **11**: 2911–2916.

[3] Takaichi K, Yagi H, Lu JR, *et al*. Highly efficient continuous-wave operation at 1030 and 1075 nm wavelengths of LD-pumped Yb^{3+}:Y_2O_3 ceramic lasers. *Appl Phys Lett* 2004, **84**: 317–319.

[4] Tokurakawa M, Shirakawa A, Ueda KI, *et al*. Continuous wave and mode-locked Yb^{3+}:Y_2O_3 ceramic thin disk laser. *Opt Express* 2012, **20**: 10847–10852.

[5] Petrov VV, Pestryakov EV, Petrov VA, *et al*. The design of Yb:Y_2O_3 ceramic diode-pumped multipass amplifier operating at cryogenic temperatures. *Laser Phys* 2014, **24**: 074014.

[6] Kim W, Villalobos G, Baker C, *et al*. Ceramic windows and gain media for high-energy lasers. *Opt Eng* 2013, **52**: 021003.

[7] Wang J, Ma J, Zhang J, *et al*. Yb:Y_2O_3 transparent ceramics processed with hot isostatic pressing. *Opt Mater* 2017, **71**: 117–120.

[8] Huang XY, Zhang X, Hu ZW, *et al*. Fabrication of Y_2O_3 transparent ceramics by hot isostatic pressing from precipitated nanopowders. *Opt Mater* 2019, **92**: 359–365.

[9] Wang J, Yin DL, Ma J, *et al*. Pump laser induced photodarkening in ZrO_2-doped Yb:Y_2O_3 laser ceramics. *J Eur Ceram Soc* 2019, **39**: 635–640.

[10] Furuse H, Nakasawa S, Yoshida H, *et al*. Transparent ultrafine Yb^{3+}:Y_2O_3 laser ceramics fabricated by spark plasma sintering. *J Am Ceram Soc* 2018, **101**: 694–702.

[11] Balabanov SS, Bykov YV, Egorov SV, *et al*. Yb:$(YLa)_2O_3$ laser ceramics produced by microwave sintering. *Quantum Electron* 2013, **43**: 396–400.

[12] Ivanov M, Kopylov Y, Kravchenko V, *et al*. Highly transparent ytterbium doped yttrium lanthanum oxide ceramics. *J Rare Earths* 2014, **32**: 254–258.

[13] Stanciu G, Gheorghe L, Voicu F, *et al*. Highly transparent Yb:Y_2O_3 ceramics obtained by solid-state reaction and combined sintering procedures. *Ceram Int* 2019, **45**: 3217–3222.

[14] Kryzhanovska OS, Baumer VN, Parkhomenko SV, *et al*. Formation peculiarities and optical properties of highly-doped $(Y_{0.86}La_{0.09}Yb_{0.05})_2O_3$ transparent ceramics. *Ceram Int* 2019, **45**: 16002–16007.

[15] Li SS, Zhu XW, Li J, *et al*. Fabrication of 5 at.% Yb:$(La_{0.1}Y_{0.9})_2O_3$ transparent ceramics by chemical precipitation and vacuum sintering. *Opt Mater* 2017, **71**: 56–61.

[16] Balabanov SS, Bykov YV, Egorov SV, *et al*. Transparent Yb:$(YLa)_2O_3$ ceramics produced by self-propagating high-temperature synthesis and microwave sintering. *Opt Mater* 2013, **35**: 727–730.

[17] Permin DA, Kurashkin SV, Novikova AV, *et al*. Synthesis and luminescence properties of Yb-doped Y_2O_3, Sc_2O_3 and Lu_2O_3 solid solutions nanopowders. *Opt Mater* 2018, **77**: 240–245.

[18] Ivanov M, Kopylov Y, Kravchenko V, *et al*. Sintering and optical quality of highly transparent Yb-doped yttrium lanthanum oxide ceramics. *Phys Status Solidi C* 2013, **10**: 940–944.

[19] Mao XJ, Li XK, Feng MH, *et al*. Cracks in transparent La-doped yttria ceramics and the formation mechanism. *J Eur Ceram Soc* 2015, **35**: 3137–3143.

[20] Yang QH, Lu SZ, Zhang B, *et al*. Preparation and laser performance of Nd-doped yttrium lanthanum oxide transparent ceramic. *Opt Mater* 2011, **33**: 692–694.

[21] Yi Q, Zhou SM, Teng H, *et al*. Structural and optical properties of Tm:Y_2O_3 transparent ceramic with La_2O_3, ZrO_2 as composite sintering aid. *J Eur Ceram Soc* 2012, **32**: 381–388.

[22] Zhu LL, Park YJ, Gan L, *et al*. Fabrication and characterization of highly transparent Er:Y_2O_3 ceramics with ZrO_2 and La_2O_3 additives. *Ceram Int* 2017, **43**: 13127–13132.

[23] Hu Y, Shahid M, Pan W. Tunable ultraviolet/visible to near-infrared down-conversion luminescence in the Er^{3+}, Yb^{3+} co-doped $(Y_{0.88}La_{0.09}Zr_{0.03})_2O_3$ transparent ceramics. *Opt Mater* 2017, **72**: 40–44.

[24] Deshmukh P, Satapathy S, Ahlawat A, *et al*. $(Yb_{0.01}Zr_{0.02}La_{0.01}Y_{0.96})_2O_3$ transparent ceramic: Fabrication, structural and optical characterization for IR emission. *J Mater Sci: Mater Electron* 2017, **28**: 11020–11028.

[25] Ning KJ, Wang J, Luo DW, *et al*. Fabrication and characterization of highly transparent Yb^{3+}:Y_2O_3 ceramics. *Opt Mater* 2015, **50**: 21–24.

[26] Zhu LL, Park YJ, Gan L, *et al*. Effects of ZrO_2–La_2O_3 co-addition on the microstructural and optical properties of transparent Y_2O_3 ceramics. *Ceram Int* 2017, **43**: 8525–8530.

[27] Chen PL, Chen IW. Grain boundary mobility in Y_2O_3: Defect mechanism and dopant effects. *J Am Ceram Soc* 1996, **79**: 1801–1809.

[28] Patel AP, Stanek CR, Levy MR, *et al*. Defect volumes of BO_2 doped Y_2O_3 (B = Ti, Zr, Hf and Ce). *Nucl Instrum Methods Phys Res, Sect B* 2010, **268**: 3111–3113.

[29] Dulina NA, Baumer VN, Danylenko MI, *et al*. Effects of phase and chemical composition of precursor on structural and morphological properties of $(Lu_{0.95}Eu_{0.05})_2O_3$ nanopowders. *Ceram Int* 2013, **39**: 2397–2404.

[30] Abramov VN, Kunznetsov AI. Fundamental absorption of Y_2O_3 and $YAlO_3$. *Sov Phys Solid State* 1978, **20**: 399–402.

[31] Ikesue A, Aung YL. Synthesis of Yb:YAG ceramics without sintering additives and their performance. *J Am Ceram Soc* 2017, **100**: 26–30.

[32] Snetkov IL, Balashov VV. Thermo-optical properties of Ho:Y_2O_3 ceramics. *Opt Mater* 2020, **100**: 109617.

[33] Wyckoff RWG. *Crystal Structures, Vol. 1*, 2nd edn. New York: John Wiley Interscience Publishers, 1963.

[34] Cantwell PR, Tang M, Dillon SJ, *et al*. Grain boundary complexions. *Acta Mater* 2014, **62**: 1–48.

[35] Bojarski SA, Ma SL, Lenthe W, *et al*. Changes in the grain boundary character and energy distributions resulting from a complexion transition in Ca-doped yttria. *Metall Mater Trans A* 2012, **43**: 3532–3538.

[36] Cantwell PR, Ma SL, Bojarski SA, *et al*. Expanding time–temperature-transformation (TTT) diagrams to interfaces: A new approach for grain boundary engineering. *Acta Mater* 2016, **106**: 78–86.

[37] Snetkov IL, Mukhin IB, Balabanov SS, *et al*. Efficient lasing in Yb:$(YLa)_2O_3$ ceramics. *Quantum Electron* 2015, **45**: 95–97.